arXiv:quant-ph/0512229v3 10 Mar 2006

Speedup of quantum state transfer by three- qubit interactions: Implementation by nuclear magnetic resonance *

Jingfu Zhang [1,2], Xinhua Peng [1], and Dieter Suter [1]

[1] *Fachbereich Physik, Universität Dortmund, 44221 Dortmund, Germany*

[2] *Department of Physics, Tsinghua University, Beijing, 100084, P R China*

(Dated: February 1, 2008)

Abstract

Universal quantum information processing requires single-qubit rotations and two-qubit interactions as minimal resources. A possible step beyond this minimal scheme is the use of three-qubit interactions. We consider such three-qubit interactions and show how they can reduce the time required for a quantum state transfer in an XY spin chain. For the experimental implementation, we use liquid-state nuclear magnetic resonance (NMR), where three-qubit interactions can be implemented by sequences of radio-frequency pulses.

PACS numbers: 03.67.Lx

* Jingfu Zhang: zhangjfu2000@yahoo.com, Jingfu@e3.physik.uni-dortmund.de
Xinhua Peng: xinhua@e3.physik.uni-dortmund.de
Dieter Suter: Dieter.Suter@uni-dortmund.de

I. INTRODUCTION

Quantum computers are capable of solving some computational problems efficiently for which no efficient classical algorithms are known. Examples include the factorization of large numbers [1], searching unsorted databases [2], and simulating quantum systems [3, 4]. While this advantage originates from a different scaling behavior compared to classical computers, rather than a higher clock speed, the time required for a single gate operation remains a critical issue: Reliable quantum computation becomes possible only if a sufficiently large number of gate operations can be completed within the decoherence time of the system.

An important element of many quantum information processing operations is the transfer of a quantum state $\alpha|0\rangle + \beta|1\rangle$ from one qubit to another [5]. We will refer to this process as quantum state transfer (QST). We thus discuss a system that is initially in state $|\Psi\rangle_i = (\alpha|0\rangle + \beta|1\rangle)_A|\psi\rangle_i$, where the qubit A is in state $\alpha|0\rangle + \beta|1\rangle$ and the other qubits in state $|\psi\rangle_i$. If we denote the QST operation as T, the state transfer from A to B can be represented as $T : |\Psi\rangle_i \rightarrow |\Psi\rangle_f = |\psi\rangle_f(\alpha|0\rangle + e^{i\phi}\beta|1\rangle)_B$: The final state corresponds to qubit B in state $\alpha|0\rangle + e^{i\phi}\beta|1\rangle$ and the other qubits in state $|\psi\rangle_f$. A quantum state transfer must thus correctly transfer the amplitudes but not necessarily the phases of the state [6]. No condition is imposed on the state of the other qubits in the system.

Currently there are three methods that can implement the QST. The first one is quantum teleportation proposed by Bennett et al [7], and has been experimentally realized in optical and liquid-state nuclear magnetic resonance (NMR) systems [8, 9]. This method is based on quantum entanglement and requires quantum measurements. Classical communication is also needed if one wants to determine the phase factor in the final state of qubit B. The second method is based on swap operations, where T can be represented as $T = \Pi S_{jl}$. S_{jl} denotes a SWAP gate that exchanges the states of qubits j and l. To realize S_{jl}, one needs external operations to control the qubits other than qubits j and l, such as switching on and off the couplings between qubits j or l and the other qubits.

The third method uses a static spin-network [6, 10]: the qubits are linearly connected by Heisenberg interactions. Qubit A is initialized into state $\alpha|0\rangle + \beta|1\rangle$ and the other qubits each into state $|0\rangle$. Under the influence of a suitable static coupling network, the system evolves such that qubit B ends up in state $\alpha|0\rangle + e^{i\phi}\beta|1\rangle$. Unlike the second method, the third method does not require spin couplings to be switched on and off, so that it is one

kind of quantum computations with the 'always on' interactions [11] that avoids single-qubit operations. Hence it is easy to implement in some solid-state systems [12]. In this article we concentrate on the third method. For example, the QST can be implemented in a three-spin linear chain with the XY- interactions $\sigma_x^1\sigma_x^2 + \sigma_y^1\sigma_y^2 + \sigma_x^2\sigma_x^3 + \sigma_y^2\sigma_y^3$.

The initial state is chosen as $(\alpha|0\rangle + \beta|1\rangle)_A|00\rangle$ by setting spin 1 at the location A into state $\alpha|0\rangle + \beta|1\rangle$ and the other spins into state $|00\rangle$. Waiting for a period of time $t_0 = \frac{\pi}{2\sqrt{2}}$, one obtains the state $|00\rangle(\alpha|0\rangle - \beta|1\rangle)_B$, which means that the spin 3 at location B is now in state $\alpha|0\rangle - \beta|1\rangle$. Both the initial state and the final state are product state. However the middle state can be an entangled states. The relation between quantum entanglement and the QST in the spin-network has been well discussed in Ref. [13]. In the three spin chain the maximum transfer distance is 2. If one transfers a state over longer distance, one needs to design and generate the couplings between spins in a linear chain, or expand the chain into a spin network through introducing the additional spins. The details can be found in Refs. [6].

Like other quantum information processing tasks, QST can be effected with a minimum set of gates [14], typically consisting of single- qubit rotations and CNOT gates that can be implemented through two- qubit interactions [4, 15]. An additional possible resource are three- spin interactions [16]. Effective three-particle interactions exist in some real physical systems, for example in optical lattices constructed of equilateral triangles [17]. The spin Heisenberg chain with three-spin interactions can exhibit interesting phase transition phenomena, such as incommensurate phases [18, 19], chiral phase transitions [20], or a quantum entanglement phase transition[21, 22].

The three- spin interaction that we consider corresponds to a coupling between next-nearest- neighbors controlled by the middle spin [17]. It is a rare resource in some quantum systems. In this article, we use the three- spin interactions in the spin XY- chain to increase the speed of the QST, and quantitatively describe the advantages obtained by using such a resource.

While nature does not provide three-spin interactions between nuclear spins, they can be simulated quite readily in liquid-state NMR [23]. For this purpose, one combines the natural two-spin interactions of the type $J_{mn}\sigma_z^m\sigma_z^n$, where σ_z^m denotes the z- component of the Pauli matrix for spin m, and J_{mn} denotes the coupling constant between spins m and n. In this work, we use this approach to generate an effective Hamiltonian with variable three-qubit

coupling strength to assess the speed-up of the QST due to three-qubit interactions.

II. XY SPIN CHAIN WITH THREE-SPIN INTERACTIONS

A. System and hamiltonian

To test the speed-up of a state-transfer operation by three-spin interactions, we consider a three spin XY chain, which is described by the Hamiltonian

$$H_{XY3} = (\sigma_x^1\sigma_x^2 + \sigma_y^1\sigma_y^2 + \sigma_x^2\sigma_x^3 + \sigma_y^2\sigma_y^3) + \frac{\lambda}{2}(\sigma_x^1\sigma_z^2\sigma_y^3 - \sigma_y^1\sigma_z^2\sigma_x^3). \tag{1}$$

Here, $\sigma_{x/y/z}^j (j = 1, 2, 3)$ are the Pauli matrices and we have set $\hbar$ and the coupling constant for the two-spin terms to one. To find an analytical expression for the time evolution of this system and determine the conditions for state transfer, we write the Hamiltonian (1) as a sum of two commuting parts, $H_{XY3} = C + D$, where

$$C = \sigma_x^1\sigma_x^2 + \sigma_y^2\sigma_y^3 + \frac{\lambda}{2}\sigma_x^1\sigma_z^2\sigma_y^3, \qquad D = \sigma_y^1\sigma_y^2 + \sigma_x^2\sigma_x^3 - \frac{\lambda}{2}\sigma_y^1\sigma_z^2\sigma_x^3. \tag{2}$$

B. Propagator and transfer speed

This decomposition shows directly that this Hamiltonian generates a periodic time-evolution: defining $k = \sqrt{2 + \frac{\lambda^2}{4}}$, we find $C^2 = D^2 = k^2 I$ and therefore

$$U(t) = e^{-iH_{XY3}t} = e^{-itC}e^{-itD} = [\cos(kt)I - i\frac{\sin(kt)}{k}C][\cos(kt)I - i\frac{\sin(kt)}{k}D]. \tag{3}$$

For times $t = n\tau = n\pi/k$ (n integer), the propagator returns to unity, $U(\tau) = I$.

The matrix representation of the propagator is

$$U(t) = \begin{pmatrix} 1 & 0 & 0 & 0 & 0 & 0 & 0 & 0 \\ 0 & \frac{(2kc)^2-(\lambda s)^2}{4k^2} & -i\frac{2kcs+\lambda s^2}{k^2} & 0 & \frac{k\lambda cs-2s^2}{k^2} & 0 & 0 & 0 \\ 0 & -i\frac{2kcs-\lambda s^2}{k^2} & \frac{k^2-4s^2}{k^2} & 0 & -i\frac{2kcs+\lambda s^2}{k^2} & 0 & 0 & 0 \\ 0 & 0 & 0 & \frac{(2kc)^2-(\lambda s)^2}{4k^2} & 0 & -i\frac{2kcs-\lambda s^2}{k^2} & -\frac{2s^2+k\lambda cs}{k^2} & 0 \\ 0 & -\frac{2s^2+k\lambda cs}{k^2} & -i\frac{2kcs-\lambda s^2}{k^2} & 0 & \frac{(2kc)^2-(\lambda s)^2}{4k^2} & 0 & 0 & 0 \\ 0 & 0 & 0 & -i\frac{2kcs+\lambda s^2}{k^2} & 0 & \frac{k^2-4s^2}{k^2} & -i\frac{2kcs-\lambda s^2}{k^2} & 0 \\ 0 & 0 & 0 & \frac{k\lambda cs-2s^2}{k^2} & 0 & -i\frac{2kcs+\lambda s^2}{k^2} & \frac{(2kc)^2-(\lambda s)^2}{4k^2} & 0 \\ 0 & 0 & 0 & 0 & 0 & 0 & 0 & 1 \end{pmatrix}, \tag{4}$$

where $c \equiv \cos(kt)$, and $s \equiv \sin(kt)$.

The propagator generates a state transfer at times $t_{QST} = \arcsin\sqrt{\frac{8+\lambda^2}{8+2\lambda^2}}/k$: If $\lambda \geq 0$, it effects a transfer from qubit 3 to qubit 1, for negative 3-qubit coupling constant in the opposite direction. In both cases, the periodicity of the overall evolution implies that the reverse transfer occurs at time $t = \pi/k - t_{QST}$. The corresponding propagators are

$$U(t_{QST_{1\to 3}}) = \begin{pmatrix} 1 & 0 & 0 & 0 & 0 & 0 & 0 & 0 \\ 0 & 0 & 0 & 0 & -1 & 0 & 0 & 0 \\ 0 & i\frac{4\lambda}{\lambda^2+4} & \frac{\lambda^2-4}{\lambda^2+4} & 0 & 0 & 0 & 0 & 0 \\ 0 & 0 & 0 & 0 & 0 & i\frac{4\lambda}{\lambda^2+4} & \frac{\lambda^2-4}{\lambda^2+4} & 0 \\ 0 & \frac{\lambda^2-4}{\lambda^2+4} & i\frac{4\lambda}{\lambda^2+4} & 0 & 0 & 0 & 0 & 0 \\ 0 & 0 & 0 & 0 & 0 & \frac{\lambda^2-4}{\lambda^2+4} & i\frac{4\lambda}{\lambda^2+4} & 0 \\ 0 & 0 & 0 & -1 & 0 & 0 & 0 & 0 \\ 0 & 0 & 0 & 0 & 0 & 0 & 0 & 1 \end{pmatrix}. \tag{5}$$

for the transfer $1 \to 3$ and

$$U(t_{QST_{3\to 1}}) = \begin{pmatrix} 1 & 0 & 0 & 0 & 0 & 0 & 0 & 0 \\ 0 & 0 & -i\frac{4\lambda}{\lambda^2+4} & 0 & \frac{\lambda^2-4}{\lambda^2+4} & 0 & 0 & 0 \\ 0 & 0 & \frac{\lambda^2-4}{\lambda^2+4} & 0 & -i\frac{4\lambda}{\lambda^2+4} & 0 & 0 & 0 \\ 0 & 0 & 0 & 0 & 0 & 0 & -1 & 0 \\ 0 & -1 & 0 & 0 & 0 & 0 & 0 & 0 \\ 0 & 0 & 0 & -i\frac{4\lambda}{\lambda^2+4} & 0 & \frac{\lambda^2-4}{\lambda^2+4} & 0 & 0 \\ 0 & 0 & 0 & \frac{\lambda^2-4}{\lambda^2+4} & 0 & -i\frac{4\lambda}{\lambda^2+4} & 0 & 0 \\ 0 & 0 & 0 & 0 & 0 & 0 & 0 & 1 \end{pmatrix} \tag{6}$$

for the transfer $3 \to 1$.

Figure 1 shows the dependence of the QST time on the strength λ of the three-qubit interaction. The overall cycle time τ decreases monotonically when a three-body coupling is added to the Hamiltonian. However, for $\lambda \neq 0$, the state transfer is no longer a simple SWAP operation, which exchanges the states of qubits 1 and 3, but the transfer becomes asymmetric, requiring different durations for the two directions. While the overall cycle time $1 \to 3 \to 1$ decreases monotonically with increasing $|\lambda|$, the slower of the two state transfers only gets faster than for $\lambda = 0$ when $|\lambda| > 2.71199$.

C. State transfer

To demonstrate the state transfer, we set qubit 1 into a superposition state $\alpha|0\rangle + \beta|1\rangle$, with the other two qubits in state $|00\rangle$. Applying the forward state transfer Eq. (5) to this state gives

$$U(t_{QST_{1\to 3}})(\alpha|0\rangle + \beta|1\rangle)|00\rangle = |00\rangle(\alpha|0\rangle - \beta|1\rangle) \tag{7}$$

and similar for the reverse transfer.

If we write this transfer in density operator notation, it reads

$$\begin{pmatrix} |\alpha|^2 & \alpha\beta^* \\ \alpha^*\beta & |\beta|^2 \end{pmatrix} \bigotimes \begin{pmatrix} 1 & 0 & 0 & 0 \\ 0 & 0 & 0 & 0 \\ 0 & 0 & 0 & 0 \\ 0 & 0 & 0 & 0 \end{pmatrix} \to \begin{pmatrix} 1 & 0 & 0 & 0 \\ 0 & 0 & 0 & 0 \\ 0 & 0 & 0 & 0 \\ 0 & 0 & 0 & 0 \end{pmatrix} \bigotimes \begin{pmatrix} |\alpha|^2 & -\alpha\beta^* \\ -\alpha^*\beta & |\beta|^2 \end{pmatrix}. \tag{8}$$

This result differs when the second and third qubits are initially in different states:

$$\begin{pmatrix} |\alpha|^2 & \alpha\beta^* \\ \alpha^*\beta & |\beta|^2 \end{pmatrix} \bigotimes \begin{pmatrix} 0 & 0 & 0 & 0 \\ 0 & 1 & 0 & 0 \\ 0 & 0 & 0 & 0 \\ 0 & 0 & 0 & 0 \end{pmatrix} \to \begin{pmatrix} 0 & 0 & 0 & 0 \\ 0 & \frac{16\lambda^2}{(\lambda^2+4)^2} & i\frac{4\lambda(\lambda^2-4)}{(\lambda^2+4)^2} & 0 \\ 0 & -i\frac{4\lambda(\lambda^2-4)}{(\lambda^2+4)^2} & \frac{(\lambda^2-4)^2}{(\lambda^2+4)^2} & 0 \\ 0 & 0 & 0 & 0 \end{pmatrix} \bigotimes \begin{pmatrix} |\alpha|^2 & \alpha\beta^* \\ \alpha^*\beta & |\beta|^2 \end{pmatrix} \tag{9}$$

$$\begin{pmatrix} |\alpha|^2 & \alpha\beta^* \\ \alpha^*\beta & |\beta|^2 \end{pmatrix} \bigotimes \begin{pmatrix} 0 & 0 & 0 & 0 \\ 0 & 0 & 0 & 0 \\ 0 & 0 & 1 & 0 \\ 0 & 0 & 0 & 0 \end{pmatrix} \to \begin{pmatrix} 0 & 0 & 0 & 0 \\ 0 & \frac{(\lambda^2-4)^2}{(\lambda^2+4)^2} & -i\frac{4\lambda(\lambda^2-4)}{(\lambda^2+4)^2} & 0 \\ 0 & i\frac{4\lambda(\lambda^2-4)}{(\lambda^2+4)^2} & \frac{16\lambda^2}{(\lambda^2+4)^2} & 0 \\ 0 & 0 & 0 & 0 \end{pmatrix} \bigotimes \begin{pmatrix} |\alpha|^2 & \alpha\beta^* \\ \alpha^*\beta & |\beta|^2 \end{pmatrix} \tag{10}$$

$$\begin{pmatrix} |\alpha|^2 & \alpha\beta^* \\ \alpha^*\beta & |\beta|^2 \end{pmatrix} \bigotimes \begin{pmatrix} 0 & 0 & 0 & 0 \\ 0 & 0 & 0 & 0 \\ 0 & 0 & 0 & 0 \\ 0 & 0 & 0 & 1 \end{pmatrix} \to \begin{pmatrix} 0 & 0 & 0 & 0 \\ 0 & 0 & 0 & 0 \\ 0 & 0 & 0 & 0 \\ 0 & 0 & 0 & 1 \end{pmatrix} \bigotimes \begin{pmatrix} |\alpha|^2 & -\alpha\beta^* \\ -\alpha^*\beta & |\beta|^2 \end{pmatrix}. \tag{11}$$

The phase of the superposition in the transferred state contains thus information on the state of the other qubits.

D. Mixed states and parallel implementation

These different cases can be implemented in parallel by using a mixed initial state [24]. By choosing $\alpha = \beta = 1/\sqrt{2}$ and adding the four initial states in Eqs. (8-11), we obtain

$$\frac{1}{2}\begin{pmatrix} 1 & 1 \\ 1 & 1 \end{pmatrix} \bigotimes \begin{pmatrix} 1 & 0 & 0 & 0 \\ 0 & 1 & 0 & 0 \\ 0 & 0 & 1 & 0 \\ 0 & 0 & 0 & 1 \end{pmatrix} = \frac{1}{2}(\sigma_x^1 + I^1) \otimes I^2 \otimes I^3.$$

In the following, we will ignore the unit operator on qubits that are in a superposition state. The state transfer acting on this initial state generates then

$$U(t_{QST_{1\to 3}})\sigma_x^1 I^2 I^3 U(t_{QST_{1\to 3}})^\ddagger = -\sigma_z^1\sigma_z^2\sigma_x^3 \tag{12}$$

For related initial conditions, we find

$$U(t_{QST_{1\to 3}})\sigma_y^1 I^2 I^3 U(t_{QST_{1\to 3}})^\ddagger = -\sigma_z^1\sigma_z^2\sigma_y^3 \tag{13}$$

$$U(t_{QST_{1\to 3}})\sigma_z^1 I^2 I^3 U(t_{QST_{1\to 3}})^\ddagger = I^1 I^2 \sigma_z^3. \tag{14}$$

Obviously the different phases that we found in the state transfer for the pure initial states result in the introduction of correlations when a mixed initial state is used. Only if the initial state is not a superposition state (Eq. 14), do we find a state transfer that does not entangle the transferred state with the other states.

III. IMPLEMENTATION IN AN NMR QUANTUM COMPUTER

The nuclear spin system that we use to implement the stepped-up QST has the natural Hamiltonian

$$H = -\pi \sum_{i=1}^{3} \nu_i \sigma_z^i + \frac{\pi}{2} J_{12}\sigma_z^1\sigma_z^2 + \frac{\pi}{2} J_{23}\sigma_z^2\sigma_z^3 \tag{15}$$

where ν_i denotes the resonance frequency of spin i. Considering this system as a quantum simulator of the Heisenberg spin chain described by the Hamiltonian (1), we generate an effective evolution (3) by an appropriate sequence of radio frequency pulses. While it is relatively straightforward to generate each of the terms of the Hamiltonian (1), they do not commute with each other. A sequential generation of the different terms therefore does not

produce the correct overall evolution. Two different approaches allow one to generate such an evolution:

- Each term is implemented for a very short duration. In this limit, the corresponding propagators are close to the unit operator and the noncommuting terms appear only in second order [25].
- The evolutions $U_C(t) = e^{-itC}$ and $U_D(t) = e^{-itD}$ are written as a product such that each factor can be implemented directly.

For the purpose of this paper, we have chosen the second approach.

A. Decomposing $U(t)$

A suitable decomposition of $U_C(t)$ uses the three operators $L_x^C \equiv \sigma_x^1\sigma_x^2/2$, $L_y^C \equiv \sigma_y^2\sigma_y^3/2$, and $L_z^C \equiv \sigma_x^1\sigma_z^2\sigma_y^3/2$. These operators can be viewed as the three components of an angular momentum vector $\mathbf{L^C}$, because they satisfy the cyclic commutation relations $[L_x^C, L_y^C] = iL_z^C$ and cycl. [26]. In terms of these operators, $U_C(t)$ becomes

$$U_C(t) = e^{-i(\frac{2\sqrt{2}}{\sin\theta_c}t)(\mathbf{L^C}\cdot\mathbf{n_c})} = e^{-i(\frac{2\sqrt{2}}{\sin\theta_c}t)(\frac{\sin\theta_c}{\sqrt{2}}L_x^C + \frac{\sin\theta_c}{\sqrt{2}}L_y^C + \cos\theta_c L_z^C)} \tag{16}$$

where $\tan\theta_c = \frac{2\sqrt{2}}{\lambda}$, and the vector $\mathbf{n_c} = (\frac{\sin\theta_c}{\sqrt{2}}, \frac{\sin\theta_c}{\sqrt{2}}, \cos\theta_c)$ gives the direction of the rotation axis for $U_C(t)$, as shown in Figure 2. Using angular momentum theory, we rewrite this as

$$U_C(t) \;=\; e^{-i\frac{\pi}{4}L_z^C} e^{i(\frac{\pi}{2}-\theta_c)L_y^C} e^{-i(\frac{2\sqrt{2}}{\sin\theta_c}t)L_x^C} e^{-i(\frac{\pi}{2}-\theta_c)L_y^C} e^{i\frac{\pi}{4}L_z^C}. \tag{17}$$

In a completely analogous way, we define $L_x^D \equiv \sigma_x^2\sigma_x^3/2$, $L_y^D \equiv \sigma_y^1\sigma_y^2/2$, and $L_z^D \equiv \sigma_y^1\sigma_z^2\sigma_x^3/2$ as the three components of the angular momentum vector $\mathbf{L^D}$. In terms of these operators, U_D becomes

$$U_D(t) = e^{-itD} = e^{-i\frac{\pi}{4}L_z^D} e^{-i(\theta_d-\frac{\pi}{2})L_y^D} e^{-i(\frac{2\sqrt{2}}{\sin\theta_d}t)L_x^D} e^{i(\theta_d-\frac{\pi}{2})L_y^D} e^{i\frac{\pi}{4}L_z^D}, \tag{18}$$

where $\theta_d = \pi - \theta_c$.

While the two-spin terms L_x and L_y in Eqs. (17) and (18) are relatively easy to implement, the three-spin terms L_z are less straightforward. We re-write them as

$$e^{i\eta L_z} = e^{i\frac{\pi}{2}L_y} e^{i\eta L_x} e^{-i\frac{\pi}{2}L_y}, \tag{19}$$

where η is an arbitrary real number. Alternatively, we may transform the propagators $e^{i\eta L_z^C}$ and $e^{i\eta L_z^D}$ as

$$e^{i\eta L_z^C} = e^{i\frac{\eta}{2}\sigma_x^1\sigma_z^2\sigma_y^3} = e^{\mp i\frac{\pi}{4}\sigma_y^1}e^{\pm i\frac{\pi}{4}\sigma_x^3}e^{i\frac{\eta}{2}\sigma_z^1\sigma_z^2\sigma_z^3}e^{\pm i\frac{\pi}{4}\sigma_y^1}e^{\mp i\frac{\pi}{4}\sigma_x^3} \tag{20}$$

and

$$e^{i\eta L_z^D} = e^{i\frac{\eta}{2}\sigma_y^1\sigma_z^2\sigma_x^3} = e^{\pm i\frac{\pi}{4}\sigma_x^1}e^{\mp i\frac{\pi}{4}\sigma_y^3}e^{i\frac{\eta}{2}\sigma_z^1\sigma_z^2\sigma_z^3}e^{\mp i\frac{\pi}{4}\sigma_x^1}e^{\pm i\frac{\pi}{4}\sigma_y^3}. \tag{21}$$

and use the decomposition of $\sigma_z^1\sigma_z^2\sigma_z^3$ into one- and two-qubit operators [23]

$$e^{i\frac{\eta}{2}\sigma_z^1\sigma_z^2\sigma_z^3} = e^{i\frac{\pi}{4}\sigma_x^2}e^{-i\frac{\pi}{4}\sigma_z^1\sigma_z^2}e^{i\frac{\pi}{4}\sigma_y^2}e^{i\frac{\eta}{2}\sigma_z^2\sigma_z^3}e^{i\frac{\pi}{4}\sigma_y^2}e^{-i\frac{\pi}{4}\sigma_z^1\sigma_z^2}e^{-i\frac{\pi}{2}\sigma_y^2}e^{-i\frac{\pi}{4}\sigma_x^2}. \tag{22}$$

The expressions (20-22) are identical to the explicit forms of (19). They use only single-qubit operations $e^{i\phi\sigma_\alpha}$ and precessions under pairwise couplings, $e^{i\xi\sigma_z^i\sigma_z^k}$, which are easy to implement experimentally.

Without loss of generality, we discuss here only the case $\lambda \geq 0$. After some simplifications [4, 26, 27], Eqs. (17) and (18) can be represented as

$$\begin{aligned} U_C(t) &= e^{\mp i\frac{\pi}{4}\sigma_y^1}e^{\pm i\frac{\pi}{4}\sigma_x^3}e^{-i\frac{\pi}{8}\sigma_z^1\sigma_z^2\sigma_z^3} \\ &\times\ e^{\mp i\frac{\pi}{4}\sigma_x^2}e^{-i\frac{1}{2}[\frac{\pi}{2}-\arctan(\frac{2\sqrt{2}}{\lambda})]\sigma_z^2\sigma_z^3}e^{\pm i\frac{\pi}{4}\sigma_x^2} \\ &\times\ e^{\mp i\frac{\pi}{4}\sigma_y^2}e^{-it\sqrt{2+\frac{\lambda^2}{4}}\sigma_z^1\sigma_z^2}e^{\pm i\frac{\pi}{4}\sigma_y^2} \\ &\times\ e^{\pm i\frac{\pi}{4}\sigma_x^2}e^{-i\frac{1}{2}[\frac{\pi}{2}-\arctan(\frac{2\sqrt{2}}{\lambda})]\sigma_z^2\sigma_z^3}e^{\mp i\frac{\pi}{4}\sigma_x^2} \\ &\times\ e^{i\frac{\pi}{8}\sigma_z^1\sigma_z^2\sigma_z^3}e^{\pm i\frac{\pi}{4}\sigma_y^1}e^{\mp i\frac{\pi}{4}\sigma_x^3}, \end{aligned} \tag{23}$$

and

$$\begin{aligned} U_D(t) &= e^{\mp i\frac{\pi}{4}\sigma_x^1}e^{\pm i\frac{\pi}{4}\sigma_y^3}e^{-i\frac{\pi}{8}\sigma_z^1\sigma_z^2\sigma_z^3} \\ &\times\ e^{\mp i\frac{\pi}{4}\sigma_x^2}e^{-i\frac{1}{2}[\frac{\pi}{2}-\arctan(\frac{2\sqrt{2}}{\lambda})]\sigma_z^1\sigma_z^2}e^{\pm i\frac{\pi}{4}\sigma_x^2} \\ &\times\ e^{\pm i\frac{\pi}{4}\sigma_y^2}e^{-it\sqrt{2+\frac{\lambda^2}{4}}\sigma_z^2\sigma_z^3}e^{\mp i\frac{\pi}{4}\sigma_y^2} \\ &\times\ e^{\pm i\frac{\pi}{4}\sigma_x^2}e^{-i\frac{1}{2}[\frac{\pi}{2}-\arctan(\frac{2\sqrt{2}}{\lambda})]\sigma_z^1\sigma_z^2}e^{\mp i\frac{\pi}{4}\sigma_x^2} \\ &\times\ e^{i\frac{\pi}{8}\sigma_z^1\sigma_z^2\sigma_z^3}e^{\pm i\frac{\pi}{4}\sigma_x^1}e^{\mp i\frac{\pi}{4}\sigma_y^3}, \end{aligned} \tag{24}$$

respectively, and the three-spin terms are implemented according to Eq. (22).

B. System and pulse sequence

For the experimental implementation, we used a sample of Carbon-13 labelled trichloroethylene (TCE), dissolved in d-chloroform. Data were taken with a Bruker DRX

500 MHz spectrometer. We denote the ^{1}H nuclear spin as qubit 2 (H2), the ^{13}C directly connected to ^{1}H is denoted as qubit 1 (C1), and the other ^{13}C as qubit 3 (C3). The parameters of the system and the NMR spectra are shown in Figures 3 and 4. The difference of frequency between C1 and C3 is $\Delta\nu_{13} = 905.3$Hz. The coupling constants are $J_{13} = 103.1$Hz, $J_{12} = 200.9$Hz, and $J_{23} = 9.16$Hz. Because of the strongly coupled carbons [28] we describe the Hamiltonian of the three-qubit system as

$$H = -\pi \sum_{i=1}^{3} \nu_i \sigma_z^i + \frac{\pi}{2} J_{12} \sigma_z^1 \sigma_z^2 + \frac{\pi}{2} J_{23} \sigma_z^2 \sigma_z^3 + \frac{\pi}{2} J_{13} (\sigma_x^1 \sigma_x^3 + \sigma_y^1 \sigma_y^3 + \sigma_z^1 \sigma_z^3). \tag{25}$$

Since we use this system to simulate a linear chain with nearest neighbor and three-body interactions, we do not use the coupling between qubits 1 and 3, which represent the end of the chain.

Because our quantum register contains only one proton spin, we can implement the rotations $e^{\pm i \frac{\pi}{4} \sigma_{x/y}^2}$ by hard $\pi/2$ proton pulses, which are selective for qubit H2. We denote rotations along the $\pm x$ or $\pm y$ axis as $[\pm \frac{\pi}{2}]_{x/y}^2$. The widths of such pulses are so short that they can be considered as ideal rotations. Figures 5 show the actual pulse sequences that we used to implement U_C and U_D.

Implementing spin-selective operations on the carbon spins turned out to be difficult. We minimized experimental errors by replacing selective pulses with non-selective pulses and free precession periods [30], using, e.g.,

$$e^{\pm i \frac{\pi}{4} \sigma_x^m} = e^{\mp i \frac{\pi}{4} \sigma_y^{1,3}} e^{i \frac{\pi}{4} \sigma_z^m} e^{\pm i \frac{\pi}{4} \sigma_y^{1,3}}, \tag{26}$$

and

$$e^{\pm i \frac{\pi}{4} \sigma_y^m} = e^{\pm i \frac{\pi}{4} \sigma_x^{1,3}} e^{i \frac{\pi}{4} \sigma_z^m} e^{\mp i \frac{\pi}{4} \sigma_x^{1,3}}, \tag{27}$$

with $m = 1$ or 3. The $\pi/2$ rotations $e^{\pm i \frac{\pi}{4} \sigma_{x/y}^{1,3}}$ act on both carbon spins C1 and C3 and were realized by hard $\pi/2$ pulses. The z-rotations $e^{i \frac{\pi}{4} \sigma_z^m}$ of individual qubits were implemented by the "chemical shift rotation" method of Linden et al. [31].

The $\pm$ signs in Eqs. (23) and (24) refer to two formally different expressions that represent the same overall transformation. Implementing both forms and summing over the result turned out to be very useful for suppressing experimental artifacts arising from nonideal gate operations. When the operations U_C and U_D are concatenated, it is possible to combine the last operation of U_C with the first of U_D and realize them as a hard pulse $[-\frac{\pi}{2}]_x^{1,3}$.

C. Experimental transfer of $(|0\rangle + |1\rangle)/\sqrt{2}$

As discussed in section II B and shown in Figure 1, the transfer from qubit 3 to 1 is always speeded up by the three-spin interaction for $\lambda > 0$. We therefore start with this transfer, initializing the system to the state $(|000\rangle + |001\rangle)/\sqrt{2}$. To calculate its time evolution, we note that, according to Eq. (4), the state $|000\rangle$ is an eigenstate of the Hamiltonian, $U(t)|000\rangle = |000\rangle$. Also from Eq. (4), we find

$$U(t)|001\rangle = \frac{(2kc)^2 - (\lambda s)^2}{4k^2}|001\rangle - i\frac{2kcs - \lambda s^2}{k^2}|010\rangle - \frac{2s^2 + k\lambda cs}{k^2}|100\rangle. \tag{28}$$

We monitor the progress of the state transfer by the amplitudes of the states $|001\rangle$ and $|100\rangle$: In a superposition with state $|000\rangle$, they correspond to x- magnetization of the qubits C3 and C1, respectively.

As discussed in sections II C and II D, we can observe the transfer from the 4 initial states $|00\rangle(|0\rangle + |1\rangle)/\sqrt{2}$, $|01\rangle(|0\rangle + |1\rangle)/\sqrt{2}$, $|10\rangle(|0\rangle + |1\rangle)/\sqrt{2}$ and $|11\rangle(|0\rangle + |1\rangle)/\sqrt{2}$ to their respective final states in parallel by preparing their sum as a mixed state $I^1 I^2 \sigma_x^3$ using pulse sequence

$$[\frac{\pi}{2}]_y^2 - [grad]_z - [\frac{\pi}{2}]_x^1 - [grad]_z - [\frac{\pi}{2}]_y^3$$

where $[grad]_z$ denotes a gradient pulse along z- axis. As usual [32], we describe these mixed states in an operator notation that refers only to the traceless part of the density operator. Since $[D, \sigma_x^3] = [C, D] = 0$, the evolution of this initial condition is determined by C alone,

$$\begin{aligned} \rho_1(t) &= U(t)\sigma_x^3 U(t)^\ddagger = U_C(t)\sigma_x^3 U_C(t)^\ddagger \\ &= \frac{(2kc)^2 - (\lambda s)^2}{4k^2}\sigma_x^3 - \frac{2kcs - \lambda s^2}{k^2}\sigma_y^2\sigma_z^3 - \frac{2s^2 + k\lambda cs}{k^2}\sigma_x^1\sigma_z^2\sigma_z^3. \end{aligned} \tag{29}$$

The first and last term in Eqn.(29) correspond to directly observable magnetization. We can therefore monitor the progress of the quantum state transfer by simply recording the free induction decay (FID) signal and calculating its Fourier transform. Figures 6 show the corresponding ^{13}C NMR spectra observed before and after the QST, using TCE. The initial condition shows that the signal is concentrated on qubit C3 shown as Figures 6 (a-c). After the transfer C3 $\rightarrow$ C1, the system is in state $-\sigma_x^1\sigma_z^2\sigma_z^3$. The main signal is on qubit C1, shown as Figures 6 (d-f) corresponding to $\lambda = 0$, 1.5, and 4, respectively. The different resonance lines indicate that the magnetization on qubit C1 is aligned along the positive or negative x- axis, depending on the state of qubits H2 and C3. This agrees well with the

prediction of Eqs. (8-11). After the transfer C3 $\rightarrow$ C1 $\rightarrow$ C3, the system is in state σ_x^3. The main signal returns to qubit C3, shown as Figures 6 (g-i) corresponding to $\lambda = 0$, 1.5, and 4, respectively. The time of QST C3 $\rightarrow$ C1 is measured to be $t = 1.00$, $t = 0.62$, and $t = 0.50$, and the time of QST C3 $\rightarrow$ C1 $\rightarrow$ C3 is measured to be $t = 2.00$, $t = 1.75$, and $t = 1.13$, when $\lambda = 0$, 1.5, and 4, respectively. Here we also use t_0 as the time unit. Compared with the case of $\lambda = 0$, the speed of QST is increased by the three- spin interactions. The experimental errors mainly result from the strong coupling between the two carbons and the effects of decoherence. Moreover the imperfection of the pulses, especially the π pulses for refocusing is another error source.

Similarly the process of transferring $(|0\rangle + i|1\rangle)/\sqrt{2}$ can be observed by choosing the initial state as $I^1 I^2 \sigma_y^3$ where $\sigma_y = (|0\rangle + i|1\rangle)(\langle 0| - i\langle 1|) - I$. Using $[C, \sigma_y^3] = 0$ we then have

$$\begin{aligned}\rho_2(t) &= U(t)\sigma_y^3 U(t)^\ddagger = U_D(t)\sigma_y^3 U_D(t)^\ddagger \\ &= \frac{(2kc)^2 - (\lambda s)^2}{4k^2}\sigma_y^3 + \frac{2kcs - \lambda s^2}{k^2}\sigma_x^2\sigma_z^3 - \frac{2s^2 + k\lambda cs}{k^2}\sigma_y^1\sigma_z^2\sigma_z^3. \end{aligned} \tag{30}$$

For these initial conditions, it is thus sufficient to consider only part of the evolution operator, generating either $U_C(t)$ or $U_D(t)$.

D. General initial conditions

For other initial conditions, the full evolution operator $U(t)$ is required. As an example, we choose $I^1 I^2 \sigma_z^3$ as the initial state, and obtain

$$\begin{aligned}\rho_3(t) &= U(t)\sigma_z^3 U^\dagger(t) \\ &= \frac{(2kc)^2 - (\lambda s)^2}{4k^2}[\frac{(2kc)^2 - (\lambda s)^2}{4k^2}\sigma_z^3 - \frac{2kcs - \lambda s^2}{k^2}\sigma_x^2\sigma_y^3 + \frac{2s^2 + k\lambda cs}{k^2}\sigma_y^1\sigma_z^2\sigma_y^3] \\ &+ \frac{2kcs - \lambda s^2}{k^2}[\frac{(2kc)^2 - (\lambda s)^2}{4k^2}\sigma_y^2\sigma_x^3 + \frac{2kcs - \lambda s^2}{k^2}\sigma_z^2 + \frac{2s^2 + k\lambda cs}{k^2}\sigma_y^1\sigma_x^2] \\ &+ \frac{2s^2 + k\lambda cs}{k^2}[\frac{(2kc)^2 - (\lambda s)^2}{4k^2}\sigma_x^1\sigma_z^2\sigma_x^3 - \frac{2kcs - \lambda s^2}{k^2}\sigma_x^1\sigma_y^2 + \frac{2s^2 + k\lambda cs}{k^2}\sigma_z^1]. \end{aligned} \tag{31}$$

Noting that J_{23} is much smaller than J_{12}, one finds that U_D requires a longer time to complete than U_C. For example, when $\lambda = 1.5$, U_C requires about 340 ms for QST from C3 to C1, while U_D requires about 420 ms. The effective T_2 (T_2^*) of the current sample is measured to be $0.35s$, $0.26s$, and $0.23s$ for C1, H2, and C3, respectively. When U_D or the full U is applied, decoherence results in a significant degradation of the experimental data.

We therefore show here only the results of the simulation. For this purpose, we also neglect the small strong-coupling effects between qubits C1 and C3. The initial states are chosen as $I^1I^2\sigma_x^3$, $I^1I^2\sigma_y^3$ and $I^1I^2\sigma_z^3$ as respectively. Because the relevant terms in Eq. (31), are not directly observable, we apply readout pulses $[\frac{\pi}{2}]_y^1$ and $[\frac{\pi}{2}]_y^3$ to $\rho_3(t)$ to obtain the observable signals of C1 and C3, respectively.

Figures 7-9 show the progress of the QST. For each initial state, the results for $\lambda = 0$, 1.5, and 4 are given. The data points can be well fitted by the corresponding theoretical graphs. Points A, B, and C denote the maxima corresponding to the time of QST C3 $\rightarrow$ C1; points D, E, and F denote the maxima corresponding to the time of QST C3 $\rightarrow$ C1 $\rightarrow$ C3. Obviously the time required for the QST decreases with the increase of λ.

IV. DISCUSSION

The QST can also be implemented by a series of SWAP operations. For the three- spin chain, the state of spin 1 can be transferred to spin 3 through

$$S_{13} = S_{12}S_{23}S_{12} = \begin{pmatrix} 1 & 0 & 0 & 0 & 0 & 0 & 0 & 0 \\ 0 & 0 & 0 & 0 & 1 & 0 & 0 & 0 \\ 0 & 0 & 1 & 0 & 0 & 0 & 0 & 0 \\ 0 & 0 & 0 & 0 & 0 & 0 & 1 & 0 \\ 0 & 1 & 0 & 0 & 0 & 0 & 0 & 0 \\ 0 & 0 & 0 & 0 & 0 & 1 & 0 & 0 \\ 0 & 0 & 0 & 1 & 0 & 0 & 0 & 0 \\ 0 & 0 & 0 & 0 & 0 & 0 & 0 & 1 \end{pmatrix}. \tag{32}$$

When $\lambda = 0$ Eqs.(6) and (5) are equivalent to S_{13} (up to some phase factors), just as discussed in Ref. [26]. When $\lambda \neq 0$, however, neither Eq.(6) nor (5) is equivalent to S_{13}. The difference between the stepped-up QST and the SWAP operation comes from the three-spin interaction, which breaks the symmetry for exchanging spins 1 and 3. One can prove that when spin 1 and spin 3 are exchanged, the three- spin terms in Eq. (1) are changed from $\frac{\lambda}{2}(\sigma_x^1\sigma_z^2\sigma_y^3 - \sigma_y^1\sigma_z^2\sigma_x^3)$ to $-\frac{\lambda}{2}(\sigma_x^1\sigma_z^2\sigma_y^3 - \sigma_y^1\sigma_z^2\sigma_x^3)$. Such asymmetry can also explain why $t_{QST_{3\rightarrow 1}}$ differs from $t_{QST_{1\rightarrow 3}}$.

While we have considered here only single-qubit states, it is also possible to transfer multi-qubit states through the Heisenberg XY spin chain [6, 33], even entangled ones. Such

transfers can also be speeded up by three-spin interactions. For example, the four Bell-states $(|00\rangle \pm |11\rangle)/\sqrt{2}$, $(|01\rangle \pm |10\rangle)/\sqrt{2}$ can be transferred from spins 2 and 3 to spins 1 and 2 by

$$U(t_{QST_{1\to 3}})(|0\rangle_1|00\rangle \pm |11\rangle)_{23}/\sqrt{2} = (|00\rangle \mp |11\rangle)_{12}|0\rangle_3/\sqrt{2} \tag{33}$$

$$U(t_{QST_{1\to 3}})(|0\rangle_1|01\rangle \pm |10\rangle)_{23}/\sqrt{2} = (|01\rangle \pm |10\rangle)_{12}|0\rangle_3(\frac{\lambda^2-4}{\lambda^2+4} + i\frac{4\lambda}{\lambda^2+4})/\sqrt{2}. \tag{34}$$

Using the analysis of section II, one finds that when $\lambda < 0$, the speed of transferring the entangled states is increased by the three-spin interactions.

V. CONCLUSION

We simulated a spin XY chain with three-spin interactions, using a three qubit NMR system. Compared to the case where the system contains only two-spin interactions, the three-spin interaction increases the speed of the operation. Our results [Eqs. (6) and (5)] show that when the three- spin interactions exist, the QST is not equivalent to the SWAP operation any more. Unlike the SWAP operation, not all rows in the unitary evolution to realize the QST have only one nonzero terms.

The simulation of the XY chain with three- spin interactions offers a possible laboratory to study the problems related to three- spin interactions. Our techniques can simulate the chain with arbitrary λ. In fact λ represents the ratio of the three-body and two- body coupling constants, because we have set the two- body coupling constants to 1. In a practical sense λ can be enhanced through increasing the three-body couplings or decreasing the two-body couplings to speed up the QST. Although our results are obtained using three spin system, they are helpful for the case of more than three spins.

VI. ACKNOWLEDGMENT

We thank Prof. Guilu Long, Prof. Jiangfeng Du and Mr. Bo Chong for helpful discussions. The experiments were performed at the Interdisciplinary Center for Magnetic Resonance. This work is supported by the Alexander von Humboldt Foundation, the Na-

tional Natural Science Foundation of China under grant No. 10374010, and the DFG.

---

[1] P. W. Shor, in Proceedings of the 35th Annual Symposium on the Foundations of Computer Science, Santa Fe, NM, 1994 (IEEE Computer Society Press, New York 1994).

[2] L. K. Grover, Phys. Rev. Lett, **79**, 325(1997); L. K. Grover, *ibid.* **80**, 4329(1998); L. K. Grover, *ibid.* **85**, 1334(2000)

[3] R. P. Feynman, Int. J. Theor. Phys, **21**, 467(1982); S. Lloyd, Nature, **273**, 1073(1996); B. M. Boghosian, and W. Taylor IV, Physica D, **120**, 30(1998);

[4] R. Somma, G. Ortiz, J. E. Gubernatis, E. Knill, and R. Laflamme, Phys. Rev. A, **65**, 042323(2002)

[5] S. Bose, Phys. Rev. Lett, **91**, 207901(2003);

[6] M. Christandl, N. Datta, A. Ekert, and A. J. Landahl, Phys. Rev. Lett, **92**, 187902(2004); M. Christandl, N. Datta, T. C. Dorlas, A. Ekert, A. Kay, and A. J. Landahl, Phys. Rev. A, **71**, 032312(2005)

[7] C. H. Bennett, G. Brassard, C. Crépeau, R. Jozsa, A. Peres, and W. K. Wootters, Phys. Rev. Lett, **70**, 1895(1993)

[8] D. Bouwmeester, J. Pan, K. Mattle, M. Eibl, H. Weinfurter, and A. Zeilinger, Nature (London) **390**, 575 (1997); D. Boschi, S. Branca1, F. De Martini, L. Hardy, and S. Popescu, Phys. Rev. Lett, **80**, 1121(1998)

[9] M. A. Nielsen, E. Knill, and R. Laflamme, Nature (London), **396**, 52 (1998)

[10] P. Karbach and J. Stolze, Phys. Rev. A, **72**, 030301(R) (2005); G. D. Chiara, D. Rossini, S. Montangero, and R. Fazio, *ibid.* **72**, 012323(2005)

[11] S. C. Benjamin, and Bose, Phys. Rev. A, **70**, 032314(2004); M.-H. Yung, S. C. Benjamin, and Bose, e-print quant-ph/0508165

[12] D. P. DiVincenzo, D. Bacon, J. Kempe, G. Burkard, and K. B. Whaley, Nature, **408**, 339(2000)

[13] X.-F. Qian, Y. Li, Y. Li, Z. Song, and C. P. Sun, Phys. Rev. A, **72** 062329(2005)

[14] G. Brassarda, S. L. Braunstein, and R. Cleve, Physica D, **120**, 43(1998)

[15] D. Deutsch, Proc. R. Soc. A, **400**, 97(1985); D. Deutsch, *ibid.* **425**, 73(1989); D. Deutsch, A. Barenco, and A. Ekert, *ibid.* **449**, 669(1995); R. Cleve, A. Ekert, C. Macchiavello and M. Mosca, *ibid.* **454** 339(1998); M. J. Bremner, C. M. Dawson, J. L.Dodd, A. Gilchrist, A. W.

Harrow, D. Mortimer, M. A. Nielsen and T. J. Osborne Phys. Rev. Lett, **89** 247902(2002); A. Barenco , C. H. Bennett, R. Cleve, D. P. DiVincenzo, N. Margolus, P. Shor, T. Sleator, J. A. Smolin and H. Weinfurter, Phys. Rev. A **52**, 3457(1995); M. D. Bowdrey, J. A. Jones, E. Knill, and R. Laflamme, *ibid.* **72**, 032315(2005)

[16] R. J. Baxter, and F. Y. Wu, Phys. Rev. Lett, **31**, 1294(1973)

[17] J. K. Pachos, and M. B. Plenio, Phys. Rev. Lett, **93**, 056402(2004)

[18] A. M. Tsvelik, Phys. Rev. B, **42**, 779(1990)

[19] H. Frahm, J. Phys. A, **25**, 1417(1992)

[20] C. D'Cruz, and J. K. pachos, eprint cond-mat/0506247

[21] P. Lou, W.-C. Wu, and M.-C. Chang, Phys. Rev. B, **70**, 064405(2004)

[22] M.-F. Yang, Phys. Rev. A, **71**, 030302(R)(2005)

[23] C. H. Tseng, S. Somaroo, Y. Sharf, E. Knill, R. Laflamme, T. F. Havel, and D. G. Cory, Phys. Rev. A, **61**, 012302(1999); N. Khaneja, S. J. Glaser, and R. Brockett, *ibid.* **65**, 032301(2002); R. Somma, G. Ortiz, E. Knill, and J. Gubernatis, e-print quant-ph/0304063

[24] E. Knill and R. Laflamme, Phys. Rev. Lett. **81**, 5672 (1998); A. Datta, S. T. Flammia, and C. M. Caves, Phys. Rev. A, **72**, 042316(2005); R. Stadelhofer, D. Suter, and W. Banzhaf, *ibid.* **71**, 032345 (2005).

[25] L. M. K. Vandersypen, and I. L. Chuang, **76**, Rev. Mod. Phys, **76**, 1037(2004); X.-H. Peng, J.-F Du, and D. Suter, Phys. Rev. A, **71**, 012307 (2005)

[26] J.-F. Zhang, G. L. Long, W. Zhang, Z.-W. Deng, W.-Z. Liu, and Z.-H. Lu, Phys. Rev. A, **72**, 012331(2005)

[27] J. -F. Du, H. Li, X. -D. Xu, M. -J. Shi, J. -H. Wu, X. -Y. Zhou, R. -D. Han, Phys. Rev. A **67**, 042316(2003)

[28] C. Miquel, J. P. Paz, M. Saraceno, E. Knill, R. Laflamme, and C. Negrevergne, Nature, **418**, 59(2002)

[29] H. Geen and R. Freeman, J. Magn. Reson. (1969-1992) **93**, 93 (1991)

[30] C. A. Ryan, M. Laforest, J. C. Boileau, and R. Laflamme, Phys. Rev. A, **72**, 062317(2005); J.-F. Zhang, G. L. Long, Z.-W. Deng, W.-Z. Liu, and Z.-H. Lu, *ibid.* **70**, 062322(2004).

[31] N. Linden, B. Hervè, R. J. Carbajo, and R. Freeman, Chem. Phys. Lett, **305**, 28(1999)

[32] I. L. Chuang, N. Gershenfeld, M. G. Kubinec, and D. W. Leung, Proc. R. Soc. London, Ser. A **454**, 447(1998).

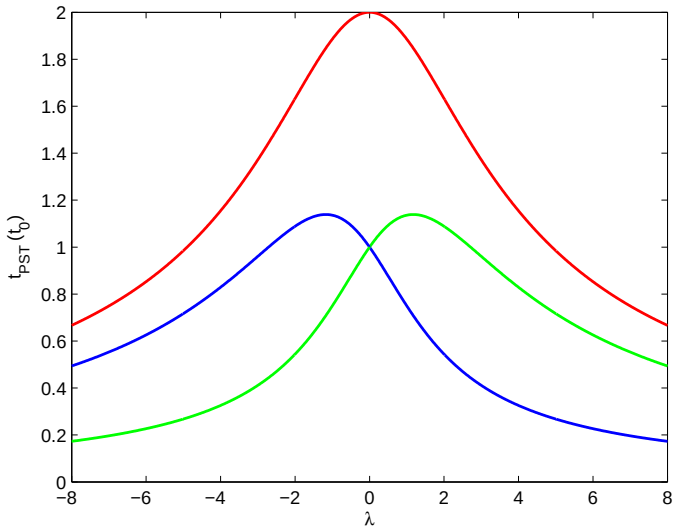

FIG. 1: (Color online) The duration of the QST $t_{QST_{1\to3}}$ (green), $t_{QST_{3\to1}}$ (blue), and $t_{QST_{3\to1\to3}}$ (red) vs λ. The unit of the vertical axes is chosen as $t_0 = \frac{\pi}{2\sqrt{2}}$, normalized to the duration for $\lambda = 0$.

[33] V. Subrahmanyam and A. Lakshminarayan, Phys. Lett. A, **349**, 164(2006)

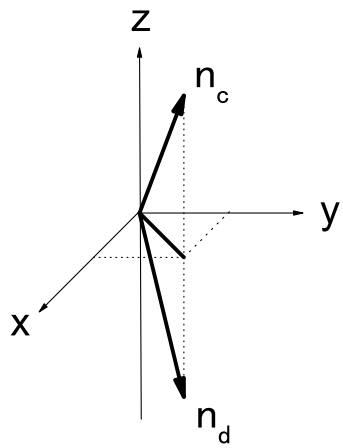

FIG. 2: The frame for operations $U_C(t)$ and $U_D(t)$. The vectors $\mathbf{n_c}$ and $\mathbf{n_d}$ denote the directions of the rotation axes for the two operations, respectively. They are tilted from the z axis by the angles θ_c and $\theta_d = \pi - \theta_c$. The projections of $\mathbf{n_c}$ and $\mathbf{n_d}$ into the xy- plane are identical and indicated by a black line. The angles between the projection and the x and y axes are $\pi/4$.

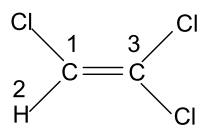

	C1	H2	C3
C1	14660.5		
H2	200.9	3232.8	
C3	103.1	9.16	15565.8

FIG. 3: The parameters of Carbon-13 labeled trichloroethylene (TCE). The diagonal terms in the table are the shifts (in Hz) of the carbons and protons with respect to the reference frequencies 500.13MHz and 125.76MHz, respectively. The non-diagonal terms are the coupling constants, also in Hz.

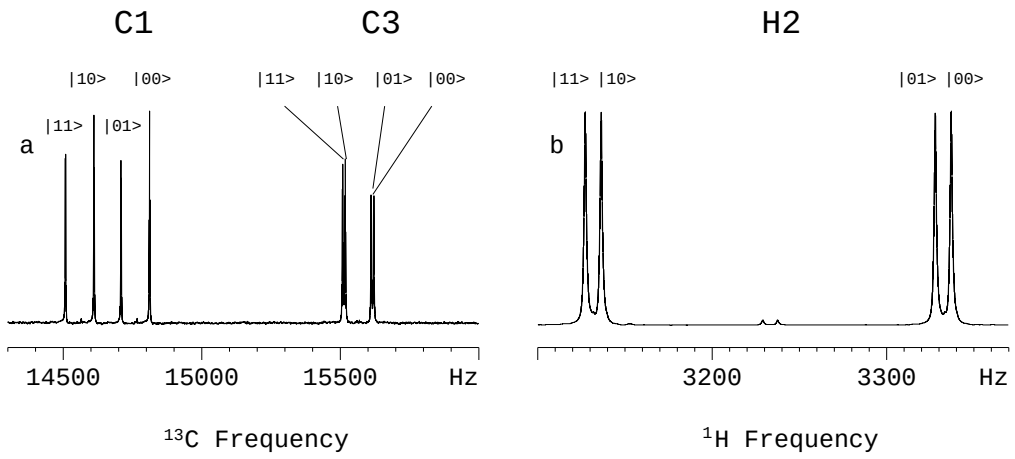

FIG. 4: The carbon spectrum (a) and proton spectrum (b) obtained by applying selective readout pulses to the system in its thermal equilibrium state. Each qubit gives rise to four resonance lines, which correspond to specific states of the other qubits. The highest frequency lines always correspond to the other qubits being in the $|00\rangle$ state, the lowest frequency lines to the $|11\rangle$ state.

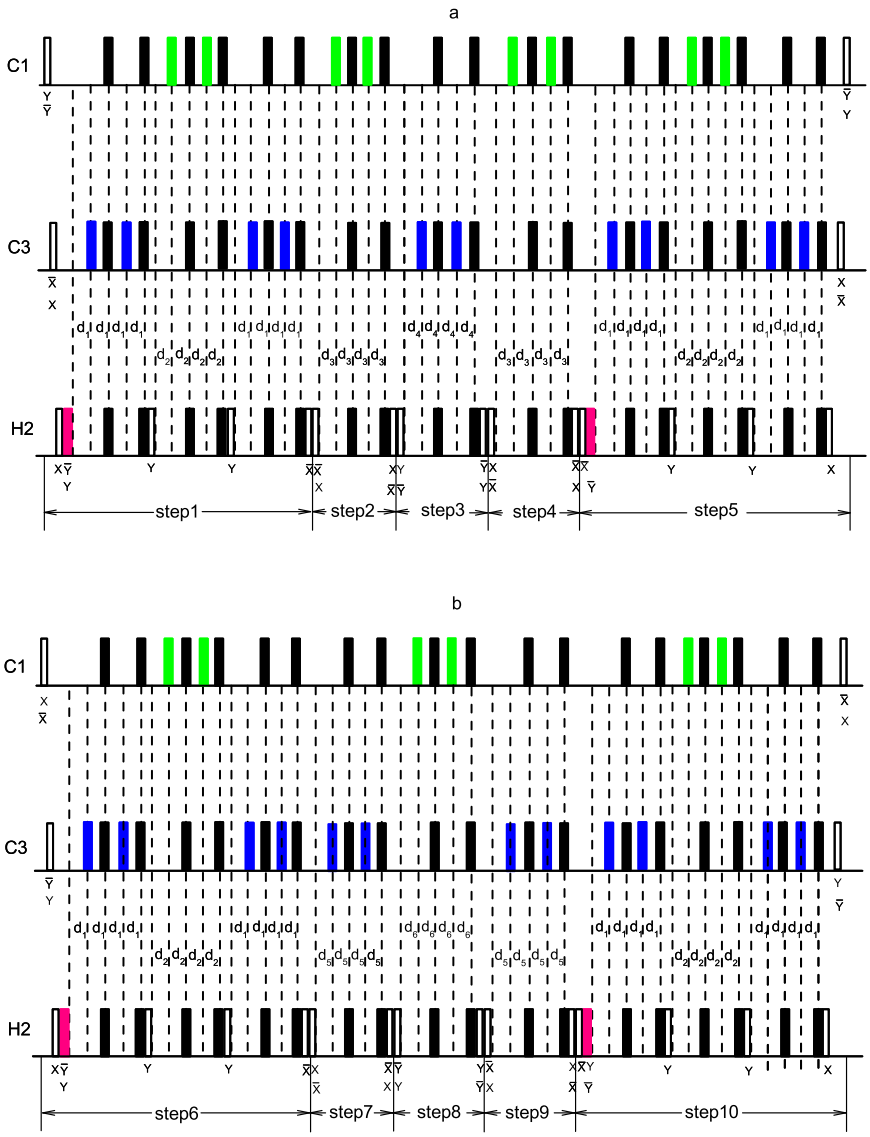

FIG. 5: Pulse sequences for the implementation of $U_C(t)$ (a) and $U_D(t)$ (b). Steps 1-10 correspond to the ten compound operations separated by '$\times$' in $U_C(t)$ and $U_D(t)$, respectively. The unfilled rectangles denote $\pi/2$ pulses, and the filled rectangles denote π pulses. X, $\overline{X}$, Y and $\overline{Y}$ below the pulses denote the x, $-x$, y, and $-y$ directions along which the pulses are applied. Those π pulses for which directions are not denoted are refocusing pulses. They are applied in pairs in which the two pulses take opposite directions to reduce experimental errors. The durations of the pulses applied to H2 and the non-selective pulses applied to C1 and C3 are so short that they can be ignored. The selective π pulses for C1 and C3, denoted by the green or blue rectangles, are implemented as RE-BURP [29] and Gauss shaped pulses with $6.2649ms$ and $2.8252ms$ durations, respectively. The delays are $d_1 = \frac{9}{8J_{12}}$, $d_2 = \frac{1}{16J_{23}}$, $d_3 = \frac{1}{4\pi J_{23}}[\frac{\pi}{2} - \arctan(\frac{2\sqrt{2}}{\lambda})]$, $d_4 = \frac{1}{2\pi J_{12}}(t\sqrt{2+\frac{\lambda^2}{4}} + 2\pi)$, $d_5 = \frac{1}{2\pi J_{12}}\{\pi - \frac{1}{2}[\frac{\pi}{2} - \arctan(\frac{2\sqrt{2}}{\lambda})]\}$, $d_6 = \frac{t}{2\pi J_{23}}\sqrt{2+\frac{\lambda^2}{4}}$. For the case of $\lambda = 0$, steps 2, 4, 7, and

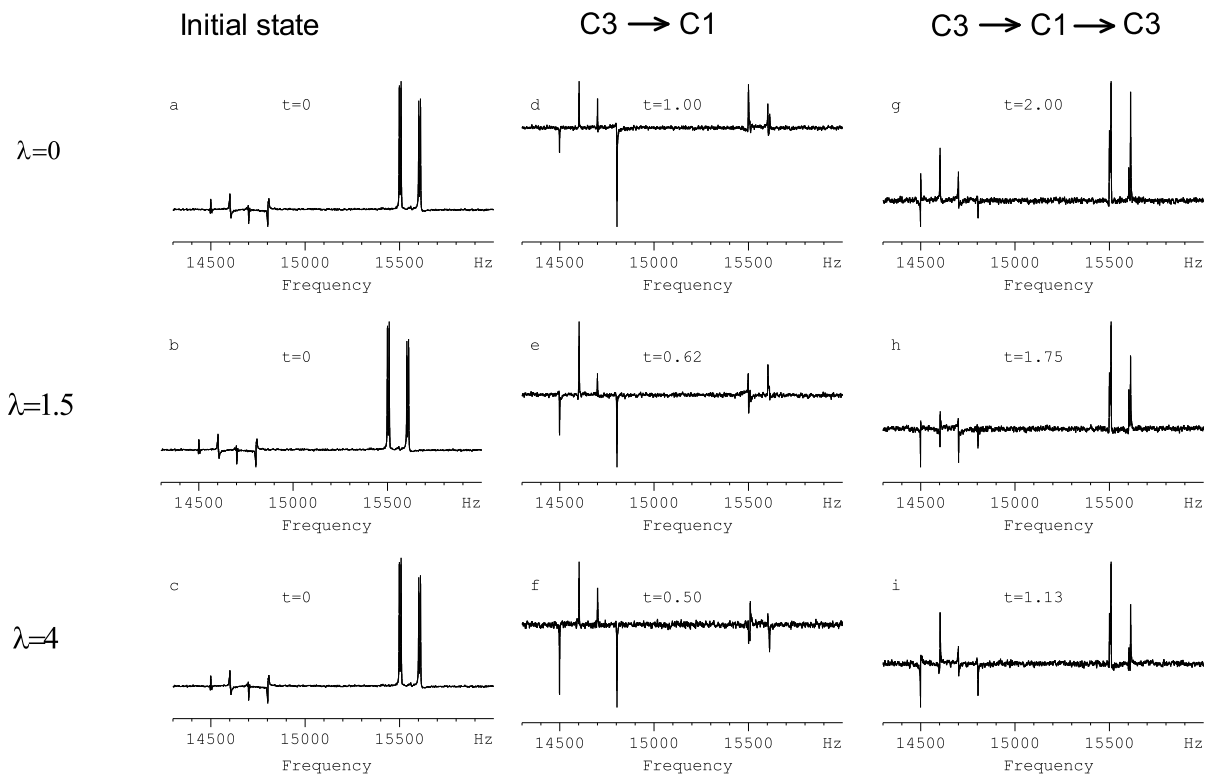

FIG. 6: The experimental results demonstrating the QST. The initial state is σ_x^3; the corresponding spectrum is shown in the left hand column. The results of the QST C3→ C1 are shown as Figures (d-f), and the results of the cyclic transfer C3 → C1 → C3 are shown as Figures (g-i). The three rows correspond to increasing three-qubit coupling strength, $\lambda = 0$, 1.5, and 4. The time required for each transfer is shown in the Figures. At $t = t_{QST_{3\to1}}$, the three-spin system is in state $-\sigma_x^1\sigma_z^2\sigma_z^3$, and at $t = t_{QST_{3\to1\to3}}$, the system is in state σ_x^3.

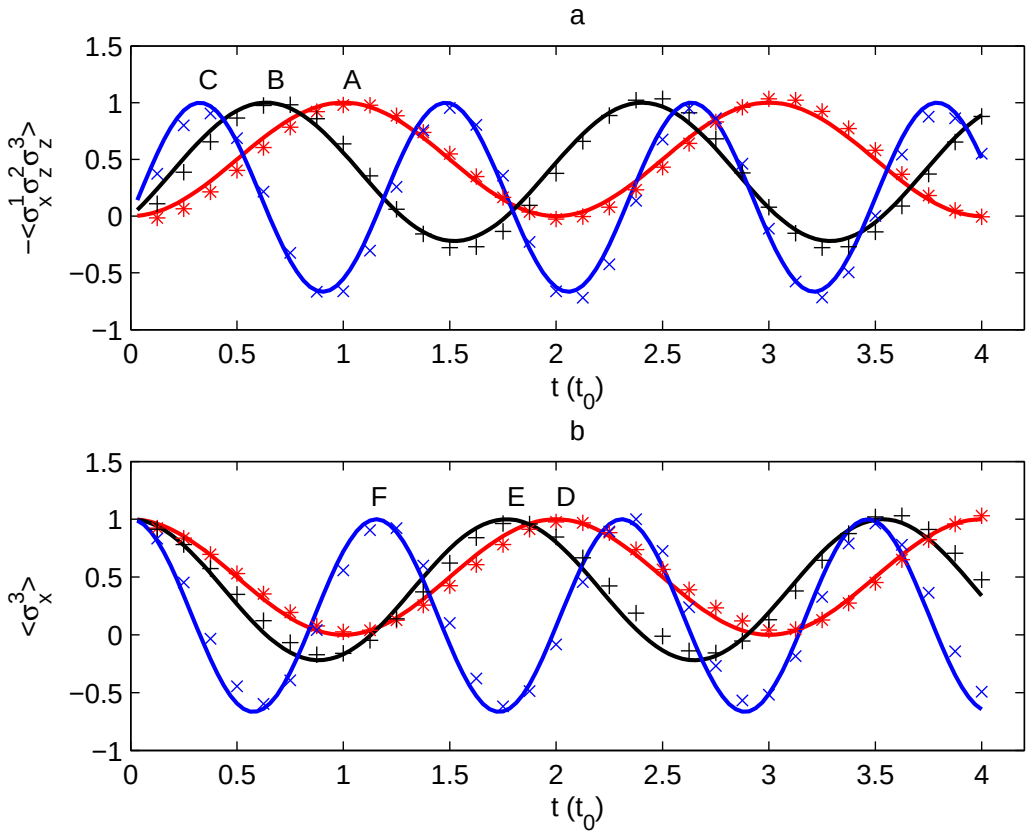

FIG. 7: (Color online) Progress of the QST, starting from σ_x^3, for different strengths of the three-body coupling. The upper part of the figure shows the overlap of the density operator with the target state $\sigma_x^1\sigma_z^2\sigma_z^3$ as a function of time. The unit t_0 of the time axis corresponds to the transfer time in the absence of the three-body interaction. The data for $\lambda = 0$, 1.5, and 4 are marked by "*", "+", and "×", respectively. The solid lines represent the theoretical results, the individual points correspond to the simulated data by setting TCE as the weak coupling system without decoherence. Points A, B, and C indicate the maxima corresponding to the transfer times C3→ C1 and the points D, E, and F to the transfer times C3 → C1 → C3. This clearly demonstrates the speedup of the transfer by the three-body interaction.

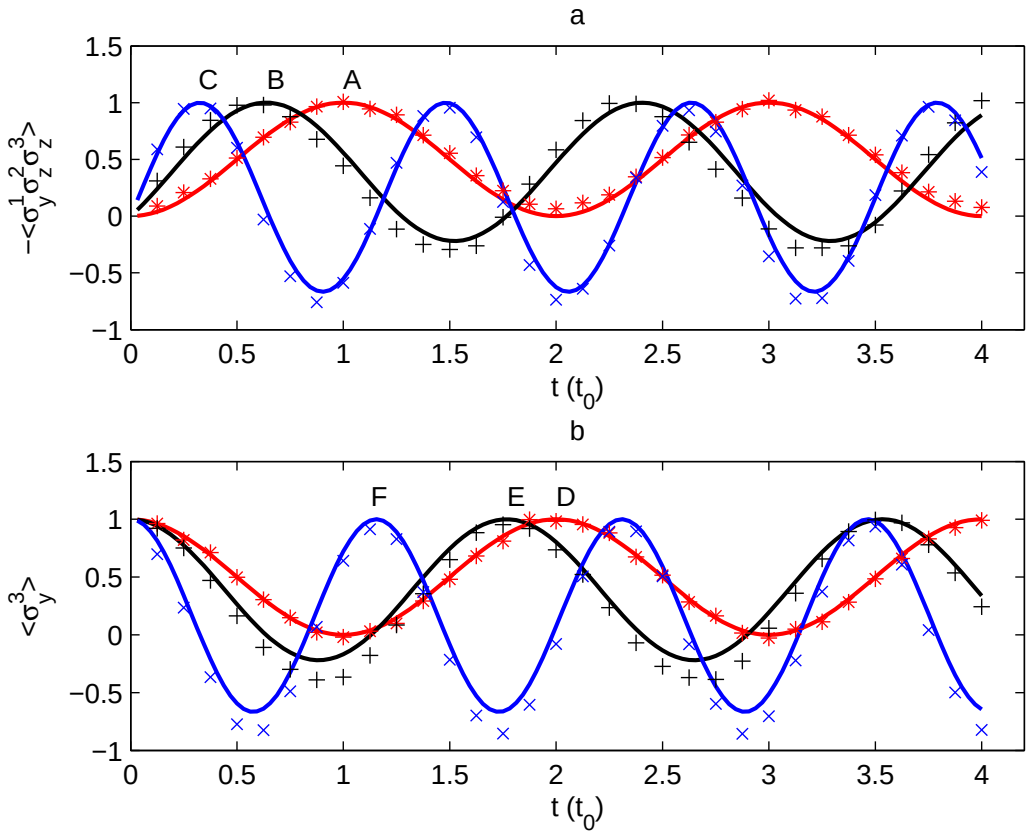

FIG. 8: (Color online) Progress of the QST, starting from σ_y^3, for different strengths of the three-body coupling. The data for $\lambda = 0$, 1.5, and 4 are marked by "*", "+", and "×", respectively. The graphs are the theoretical results, used to fit the corresponding data. Points A, B, and C indicate the maxima corresponding to the transfer times C3 → C1 and points D, E, and F to the transfer times C3 → C1 → C3.

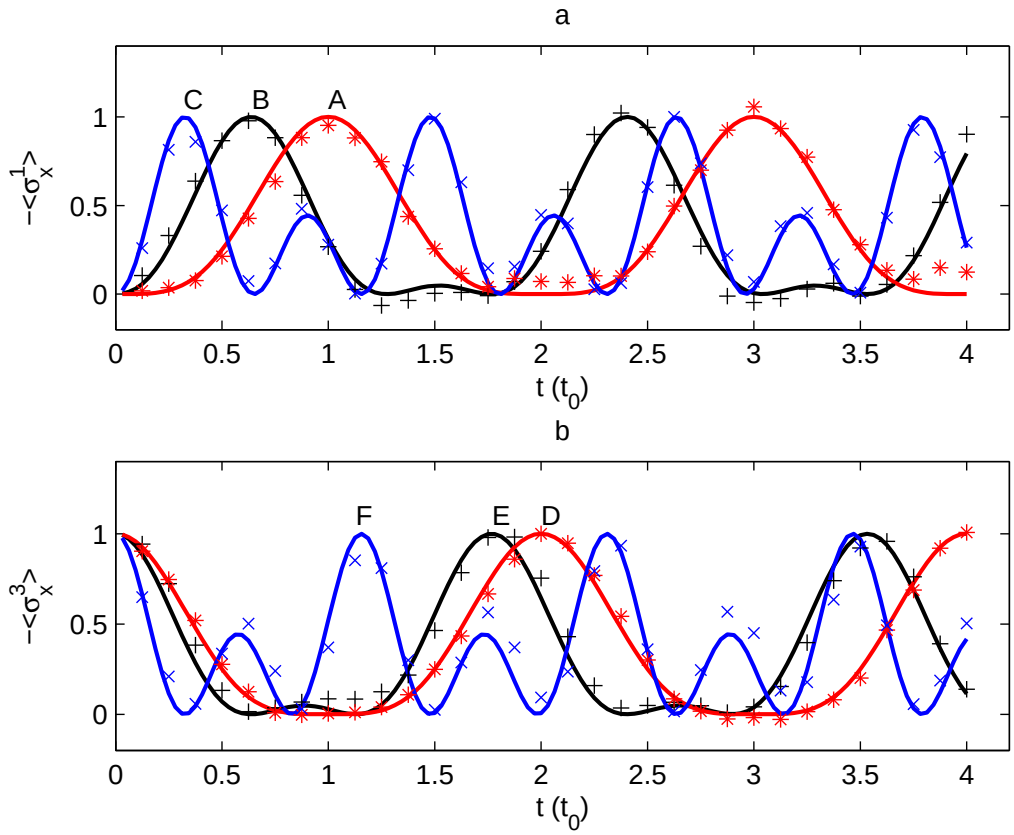

FIG. 9: (Color online) Progress of the QST, starting from σ_z^3, for different strengths of the three-body coupling. The data for $\lambda = 0$, 1.5, and 4 are marked by "*", "+", and "×", respectively. The graphs are the theoretical results, used to fit the corresponding data. Points A, B, and C indicate the maxima corresponding to the transfer times C3 → C1 and points D, E, and F to the transfer times C3 → C1 → C3.